Published in final edited form as:
Exp Neurol. 2014 November ; 0: 802–811. doi:10.1016/j.expneurol.2014.09.002.

Deletion of Olfactomedin 2 induces changes in the AMPA receptor complex and impairs visual, olfactory, and motor functions in mice

Afia Sultana[1], **Naoki Nakaya**[1], **Lijin Dong**[2], **Mones Abu-Asab**[3], **Haohua Qian**[4], and **Stanislav I. Tomarev**[1,*]

Afia Sultana: sultanaa@nei.nih.gov; Naoki Nakaya: nakayan@nei.nih.gov; Lijin Dong: Lijin.Dong@nih.gov; Mones Abu-Asab: mones@nei.nih.gov; Haohua Qian: qianh@nei.nih.gov; Stanislav I. Tomarev: tomarevs@nei.nih.gov

[1]Section on Retinal Ganglion Cell Biology, Laboratory of Retinal Cell and Molecular Biology, National Eye Institute, National Institutes of Health, Bethesda, Maryland 20892, USA

[2]Genetic Engineering Facility, National Eye Institute, National Institutes of Health, Bethesda, Maryland 20892, USA

[3]Histopathology Core Facility, National Eye Institute, National Institutes of Health, Bethesda, Maryland 20892, USA

[4]Visual Function Core, National Eye Institute, National Institutes of Health, Bethesda, Maryland 20892, USA

Abstract

Olfactomedin 2 (Olfm2) is a secretory glycoprotein belonging to the family of olfactomedin domain-containing proteins. A previous study has shown that a mutation in *OLFM2* is associated with primary open angle glaucoma in Japanese patients. In the present study, we generated *Olfm2* deficient mice by replacing the *Olfm2* gene with the *LacZ* gene. Loss of *Olfm2* resulted in no gross abnormalities. However, *Olfm2* null mice showed reduced exploration, locomotion, olfactory sensitivity, abnormal motor coordination, and anxiety related behavior. The pattern of the *Olfm2* gene expression was studied in the brain and eye using β-galactosidase staining. In the brain, *Olfm2* was mainly expressed in the olfactory bulb, cortex, piriform cortex, olfactory trabeculae, inferior and superior colliculus. In the eye expression was detected mainly in retinal ganglion cells. In *Olfm2* null mice, the amplitude of the first negative wave in the visual evoked potential test was significantly reduced as compared with wild-type littermates. Olfm2, similar to Olfm1, interacted with the GluR2 subunit of the AMPAR complexes and Olfm2 co-segregated with the AMPA receptor subunit GluR2 and other synaptic proteins in the synaptosomal membrane fraction upon biochemical fractionation of adult mice cortex and retina. Immunoprecipitation from the synaptosomal membrane fraction of *Olfm2* null mouse brain cortex using the GluR2 antibody showed reduced levels of several components of the AMPAR complex in the immunoprecipitates

*Corresponding author at: Bldg. 6, Room 212, 6 Center Drive, National Eye Institute, NIH, Bethesda, MD 20892 USA, tomarevs@nei.nih.gov. Phone: 1-301-496-8524.

including Olfm1, PSD95 and CNIH2. These results suggest that heterodimers of Olfm1 and Olfm2 interact with AMPAR more efficiently than Olfm2 homodimers and that Olfm2 plays a role in the organization of the AMPA receptor complexes.

Keywords

olfactomedin 2; AMPA receptor; neurobiology; mouse; anxiety behavior; olfactory defects; retina

Introduction

Olfactomedin 2 (Olfm2), also known as OlfC or olfactomedin-related endoplasmic reticulum-localized-2 (Noelin-2), is a secretory glycoprotein that belongs to the family of olfactomedin domain-containing proteins consisting of 13 family members in mammals (Kulkarni et al., 2000, Tomarev and Nakaya, 2009). The family of olfactomedin domain-containing proteins segregates into seven subfamilies (Zeng et al., 2005). Olfm2 together with olfactomedin 1 (Olfm1) and olfactomedin 3 (Olfm3) forms subfamily I. Genes encoding Olfm1-3 are preferentially expressed in the neuronal tissues during development and in adults (Danielson et al., 1994, Nagano et al., 2000, Torrado et al., 2002, Lee et al., 2008, Nakaya et al., 2008, Nakaya et al., 2012). Olfm1-3 show about 60% identity in the amino acid sequences and are highly conserved in evolution (Tomarev and Nakaya, 2009). Olfm2, similar to Olfm1 and Olfm3, contains a signal peptide at its N-terminus and a highly conserved olfactomedin domain at its C-terminus. Our previous study has shown that Olfm2 interacts with Olfm1 and Olfm3 (Sultana et al., 2011, Nakaya et al., 2013). Moreover, mutations in any subfamily I member inhibiting its secretion also inhibit secretion of other subfamily members (Sultana et al., 2011).

Recent proteomic studies demonstrated that Olfm1-3 are components of the AMPA-type glutamate receptor (AMPAR) complex (Schwenk et al., 2012, Shanks et al., 2012, Nakaya et al., 2013). AMPARs are the major receptors responsible for fast excitatory synaptic transmission, postsynaptic plasticity, and synapse development in the central nervous system. Available data suggest that the properties and function of the AMPAR complexes may be different depending on the particular subunit composition (Schwenk et al., 2012). The exact consequences of Olfm1 (as well as Olfm2 and Olfm3) interaction with AMPARs on their functions are still not well understood. Our recent data demonstrated that the deletion of 52 amino acids in the central part of Olfm1 dramatically reduces its interaction with Olfm2 and GluR2 and GluR4 subunits of AMPARs (Nakaya et al., 2013). Mice expressing Olfm1 with a deletion in the central part of the protein molecule demonstrated an increase in intracellular $Ca2^{+}$ concentration as well as activation of ERK1/2, MEK1 and CaMKII in the hippocampus and olfactory bulb compared with their wild-type (WT) littermates. We suggested that excessive activation of the CaMKII and Ras-ERK pathways in the Olfm1 mutant olfactory bulb and hippocampus by elevated intracellular calcium may contribute to the observed abnormal behavior and olfactory activity of Olfm1 mutant mice (Nakaya et al., 2013).

In the present study, we produced *Olfm2* knockout (KO) mice to gain greater insight into the possible functions of Olfm2 and other subfamily members. We showed that *Olfm2* loss results in no gross structural abnormalities of the brain or eye. However, *Olfm2* KO mice showed some behavioral changes and changes in the AMPA receptor complex compared with their WT littermates. We demonstrated that Olfm2 and Olfm1 are present in a synaptosomal membrane fraction (LP1) enriched in GluR2 and other synaptic membrane proteins. Elimination of Olfm2 resulted in a reduction of several AMPAR components in GluR2 antibody immunoprecipitates from the cortex LP1 fraction. Our data suggests that Olfm2, similar to Olfm1, is an important player at synapses and loss of Olfm2 may lead to neurological defects associated with behavior abnormalities.

Materials and methods

Animals

All animals used in the experiments were managed according to the ARVO statement for the use of animals in ophthalmic and vision research. All experiments using animals were approved by the NEI Animal Care and Use Committee. *Olfm1* mutant mice have been reported previously (Cheng et al., 2007, Nakaya et al., 2013). A mouse line in which the cre expression is under the control of regulatory sequences of the mouse zona pellucida 3 gene promoter (ZP3-cre) (Lewandoski et al., 1997) was obtained from the Jackson laboratory.

Generation and characterization of Olfm2 KO mice

Olfm2 KO (*Olfm2*-KO) mice were generated by deleting exons 2–6 of the *Olfm2* gene. A BAC clone containing mouse *Olfm2* locus was obtained from Geneservices (Cambridge, UK) and was used to construct a targeting vector in which exons 2–6 were replaced with the *LacZ* gene (β-galactosidase or β-gal). This targeting vector also contained a PGK neo-cassette flanked by the LoxP sites. The targeting vector was electroporated into R1 (129S6) ES cell line. Clones resistant to G418 were selected, expanded, and screened for homologous recombination using long range genomic PCR and Southern blotting. For Southern blotting of the 5′ flanking probe, genomic DNA was cleaved with ScaI to produce restriction fragments of 15.5 and 9.3 kb for the WT and KO alleles, respectively. For the 3′ flanking probe, genomic DNA was cleaved with BamHI to produce restriction fragments of 14.2 and 12.3 kb for the WT and KO alleles, respectively. Further characterization of positive embryonic stem cell clones was done by karyotyping. Two positive clones were injected into the C57BL/6 mouse blastocyst. Generation of chimeric mice and germ line transmission were performed as described previously (Michalska and Choo, 1993). The selection marker LoxP-PGK-neo-LoxP was removed by mating mice with the ZP3-cre line. Genotyping of animals was performed by PCR using genomic DNA isolated from the tails of 4 week-old mice. A single PCR reaction was designed using a common forward PCR primer located in intron 1 - Olfm2C-F 5′-GCTCTGTGGATGGGTTCCTA-3′ and two reverse primers - Olfm2-WTR2 5′-GAGGCAAAAGGGAATGTCAG-3′ located in intron 2 for the WT allele and Olfm2-KOR2 5′-CTTGAGCAGCTCCTTGCTG-3′ located in *LacZ* for the targeted allele. The PCR was performed by initial denaturation at 94°C for 2 min followed by 30 cycles with denaturation at 94°C for 30 s, annealing and elongation at 60°C

for 1 min and a final elongation at 72°C for 7 minutes using TaKaRa LA Taq DNA polymerase (Takara Bio).

Quantitative RT-PCR (Q-PCR) RNA was isolated from the adult mouse brain using a Trizol reagent (Invitrogen) following the manufacturer's instructions. cDNA was synthesize using 1 μg of total RNA and a cDNA kit (Applied Biosystems Inc. ABI). Q-PCR was performed with synthesized cDNA as a template using a SYBR Green PCR master mix (ABI) and a real-time thermocycler (7900HT; ABI). *GAPDH* was used for normalization. Primers for Q-PCR have been previously described (Sultana et al., 2011). Each sample was analyzed in triplicates. Experiment was repeated twice using independent samples.

Antibody production

Purified Olfm2 was purchased from R&D systems. A polyclonal antibody generated against purified Olfm2 was produced by Covance, Inc. This antibody detected Olfm2 but not closely related Olfm1 or Olfm3 proteins expressed in HEK293 cells transiently transfected with corresponding expression constructs. A polyclonal Olfm2 peptide antibody generated against synthetic peptide RSLDARLRAADGSVSAKSF was reported previously (Sultana et al., 2011).

β-gal enzymatic assay

Postnatal and adult brains and eyes from WT, *Olfm2* heterozygous and homozygous KO mice were fixed for 30 minutes at 4°C in 4% paraformaldehyde (PFA) and washed in PBS three times for 15 min. Coronal brain slices (100 μm thick) were made using a vibratome (Vibratome Leica VT 1000 S). Slices were incubated in stain buffer containing 5 mM potassium ferricyanide, 5 mM potassium ferrocyanide, 1 mg/ml X-gal (Invitrogen) for 24–72 h at 37°C. The reactions were stopped by washing in PBS three times for 10 min. Sections were then mounted on slides, dried overnight, dehydrated through grades of alcohol, and mounted. Sections from WT mice were used as control for β-gal background staining. Some sections were counterstained with Vector nuclear fast red stain (Vector laboratories) for 5–10 min, washed for 10 min, dehydrated and mounted. Entire brains were incubated in stain buffer for whole brain staining. For retinal whole mount staining, retinas were incubated in stain buffer for 24–72 h, followed by PBS wash and flat mounting on slides. For frozen eye sections, fixed stained eyes were equilibrated in 30% sucrose, embedded in OCT compound (Electron Microscopy Sciences), 12 μm frozen sections were prepared, and counter stained with nuclear fast red stain.

Intraocular pressure measurements—IOP measurements in both the eyes of Olfm2 KO and WT littermates were measured using a handheld digital tonometer (Tonolab Icare, Helsinki, Finland) in the morning. The average value of five consecutive measurements with a deviation less the 5% was recorded.

Visual evoked potential (VEP) and electroretinogram (ERG)

Mice were anesthetized by an intraperitoneal injection of ketamine (100 mg/kg) and xylazine (9 mg/kg). Pupils were dilated with 1% tropicamide and 2.5% phenylephrine. ERG and VEP were recorded simultaneously using an Espion E2 electrophysiology system

(Diagnosys, LLC MA, USA). Two subdermal needle electrodes were placed 2 mm lateral to lambda on each side for VEP recording. Standard ERG were recorded on both eyes with a gold wire loop electrode placed in the center of the cornea, a reference electrode placed in the forehead, and a grounding electrode in the tail. White xenon flashes of 0.3–100 cd.s/m^2 in white background were generated every 0.5 sec and responses were recorded simultaneously for 0.3 sec after each stimulation. Results were averaged from 100 repetitive responses.

Optic nerve morphological analysis

Animals were perfused transcardially with a fixative containing 2% PFA and 2% glutaraldehyde. Optic nerves were carefully dissected and placed in a fixative overnight. The nerve segments were washed three times in PBS, placed in 2% osmium tetroxide for 1 h, washed with PBS, dehydrated in ethanol, and subsequently embedded in an epoxy resin. For light microscopy 1 μm thick semi thin cross sections were cut and stained with 1% toluidine blue/paraphenylenediamine. For electron microscopy analysis, 80 nm thin sections were cut. Total optic nerve cross-section area was measured using light microscopy pictures at 10x magnification and cross-section images of axons were photographed at 2,200x or 4,000x magnification.

Mouse behavioral tests

WT and homozygous 2–8 month-old *Olfm2*-KO mice were used for behavioral analysis. Animals of the same age were used for each behavioral test.

An Elevated Plus Maze Test (EMT) was carried out on five pairs of *Olfm2*-KO and WT littermates with age ranging from 5 to 8 months. H10-35-EPM system (Coulbourn Instruments, PA) was used as described previously (Lister, 1987, Park et al., 2005, Mead et al., 2006). Briefly, each mouse was placed in the central area of the plus maze and was allowed to explore different areas for 10 minutes. Each experiment was recorded using a camera connected to a computer. The time spent in each area, the number of entries made into different areas, and the latency to enter an open and closed area was calculated for each animal. Marble burying behavior was also used to test the anxiety behavior of *Olfm2*-KO and their WT littermates. Twenty green marbles were placed on the top of a 10 cm deep flake bedding in a clear mouse cage. Each animal was placed individually in a cage and kept there for 20 min. At the end of the test, marbles with more than 2/3 of their surface area covered or completely hidden by the bedding were counted (Thomas et al., 2009).

General locomotive activity was measured in the open field test as described previously (Basta-Kaim et al., 2011). Spontaneous locomotor activity was recorded by placing mice in the middle of an arena (44.5 × 44.5 cm). The distance traveled in 10 min was monitored by infrared beams using Auto-Track software (Columbus Instruments, Opto-Varimex 4). Anxiety-like behavior was tested by placing mice in the arena described above that was divided into light and dark compartments (44.5 × 22 cm each). The compartments were connected by a small opening (10 × 10 cm). Mice were placed in the light compartment and time that they spent in each compartment as well as the amount of entries into each compartment was recorded using infrared beams during the 10 min test period.

Coordinated motor activities were measured by a rotarod apparatus (Ugo-Basile, Varese, Italy). Mice were placed on an accelerating rotating rod at 4 rpm. The speed of rotation was gradually increased up to 40 rpm and the time until the mice fell to the floor was recorded. Each animal was tested three times a day for three consecutive days and the mean values were calculated.

Olfactory sensitivity of *Olfm2*-KO and WT littermates was assessed as described previously (Witt et al., 2009). Mice were individually habituated to the experimental environment by placing them sequentially in three clean, empty cages for 15 min in each cage. After habituation in the test cage, filter papers (5 × 5 cm) scented with either water or test odorant were sequentially placed in a cage for 3 min with an interval of 1 min between each odorant. Mouse behavior was recorded using a digital video camera. Exploratory time was measured in sec and defined as the time when the mouse nose was < 1 mm from the filter paper.

Subcellular fractionation, Western blot and immunoprecipitation

The cerebral cortex and retina (n=5) were isolated from WT mice and were homogenized followed by fractionation as described previously (Hallett et al., 2008). Briefly, for the synaptic membrane fraction, the dissected cortex and retina were homogenized in an ice cold buffer containing 320 mM sucrose, 10 mM Tris base, 5 mM NaF, 1mM Na_3VO_4, 1 mM EDTA, 1 mM EGTA, pH 7.4 supplemented with a protease inhibitor cocktail (Roche) and centrifuged for 10 min at 800 g at 4°C. Supernatant (S1) was collected and centrifuged for 15 min at 9,200 g at 4°C. The resultant pellet (P2) was re-suspended in a buffer containing 35.6 mM sucrose, 10 mM Tris base, 5 mM NaF,1 mM Na_3VO_4, 1 mM EDTA, 1mM EGTA, pH 7.4 supplemented with protease inhibitor cocktail, vortexed for 5–10 sec, and incubated on ice for 30 min. The re-suspended P2 pellet was then centrifuged for 20 min at 25,000 g at 4°C. Supernatant (LS1) was removed and the pellet (LP1) containing synaptosomal membrane from the cortex and the retina were re-suspended after brief washing. The LS1 and LP1 fractions were analyzed by Western blotting using antibodies against Olfm2 (peptide polyclonal 1:500 dilution), Olfm1 (monoclonal 1:2000 dilution), GluR2 (Millipore, 1:2000 dilution), PSD95 (Cell Signaling, 1:1000 dilution) and tubulin (Promega, 1:1000 dilution). The cerebral cortex was isolated from *Olfm2*-KO (n=3) and WT littermates (n=3) and was fractionated to get LP1 fraction as described above. The levels of various synaptic proteins was analyzed using antibodies against Olfm2 (polyclonal 1:500 dilution), Olfm1 (monoclonal 1:2000 dilution), GluR1, GluR3 and CNIH2 (Synaptic Systems, 1:2000 dilution), GluR4, GluR2, pGluR2 and synaptophysin (Millipore, 1:2000 dilution), PSD95, PKCα (Cell Signaling, 1:1000 dilution), synaptogyrin3 (Abcam 1:1000) and tubulin (Promega, 1:1000 dilution). For co-immunopreciptation experiments, the LP1 fractions from *Olfm2* KO, and *Olfm1* mutant along with WT littermates were used. Briefly, the LP1 fractions were first treated with protein G at 4°C for 3 h to reduce the background followed by centrifugation to pellet the agarose G beads. The supernatant LP1 fraction was then incubated for 1 h with 0.5 μg of polyclonal antibodies against Olfm1, GluR2 (Millipore) or control IgG at 4°C. 50 μl of homogeneous protein G beads suspension blocked with 0.05% BSA was added to the mixture and incubated overnight at 4°C on a rotator. Protein G beads were collected by centrifugation, washed three times with lysis buffer and bound proteins were eluted and analyzed by Western blotting using antibodies

against Olfm2 (1:500 dilution), GluR2 (1:2000 dilution), CNIH2 (1:2000), PSD95 (1:1000), and Olfm1 (monoclonal,1:2000 dilution).

Statistical analysis

Data from various experiments were analyzed using a student's unpaired t test.

Results

Targeted deletion of Olfm2

To gain insight into possible functions of the *Olfm2* gene, we produced *Olfm2*-KO mice through homologous recombination in ES cells. The mouse *Olfm2* gene has 6 exons with the translation initiation site located in exon 1. We generated a targeting vector by replacing exon 2–6 of the *Olfm2* gene with the *LacZ* reporter gene and the neo-selection cassette flanked by the loxP sites (Fig. 1A). PCR analysis and southern blots (Fig. 1B) were used to select ES clones with an accurate site-specific recombination. Two correctly recombined R1 ES clones were injected into mouse blastocysts to obtain chimeric mice, which were then backcrossed with C57BL/6 females to obtain F1 mice with germline transmission of the KO allele. One line was selected for further analysis. A single genotyping PCR assay was performed to detect the presence of the WT allele (280bp) and the KO allele (744bp) (Fig. 1C). F1 mice were mated to homozygosity to produce *Olfm2*-KO mice (*Olfm2*-KO^{LacZ}) that lacked *Olfm2* mRNA transcripts as analyzed by Q-PCR. *Olfm2*-KO^{LacZ} homozygous mice were crossed with the ZP3-cre line, a female germline cell specific Cre line (Lewandoski et al., 1997), to eliminate the neo-selection cassette. *Olfm2*-KO^{LacZ} mice had normal life span and didn't show gross phenotypic defects. No postnatal lethality was observed (Fig. 1D) and no difference was found in the body weight between *Olfm2*-KO^{LacZ} mice and their WT littermates (Fig. 1E).

Olfm2 expression in neuronal tissues

Olfm2-KO^{LacZ} mice were used to study the expression of *Olfm2* in the brain and eye. Whole brain and its coronal vibrotome sections from P1, P5, P13 and adult *Olfm2*-KO^{LacZ} mice and their WT littermates were stained for a β-gal activity. Expression of *Olfm2* was detected in the developing cortex at P1 (not shown) and increased by P5. At P5, expression was mainly localized to motor cortex, primary visual area, and primary somatosensory area (Fig. 2A–B) on the dorsal side of the brain. The ventral side of the brain showed expression of *Olfm2* in the anterior olfactory nucleus, piriform cortex, and pontine nucleus (Fig. 2C). Vibratome sections of the P5 mouse olfactory bulb showed *Olfm2* expression in the glomerular layer, mitral cell layer, and accessory olfactory bulb (Fig. 2D). Strong expression of *Olfm2* was also detected in the piriform cortex and olfactory trabeculae (Fig. 2E–F). *Olfm2* pattern of expression in the adult brain was similar to that at P5. *Olfm2* was expressed mainly in the motor cortex (M1), primary visual area (V1), and primary somatosensory area (S1). In addition, expression of *Olfm2* was also detected in the superior and inferior colliculus (Fig. 2G). Vibratome sections of the adult brain showed *Olfm2* expression in the glomerular layer (GL), mitral cell layer (MCL), and anterior olfactory nucleus (AON) (Fig. 2H). In the adult cortex, expression was mainly detected in layers II–IV (Fig. 2I). In the eye, *Olfm2* was expressed in the differentiating and adult retinal ganglion cells (RGCs) (Fig. 3A–F). *Olfm2*

expression level in RGCs was stronger at early postnatal stages than in adults. At embryonic day 18.5, the earliest developmental stage tested, low level of *Olfm2* expression was also detected in the optic nerve (data not shown). In general, pattern of *Olfm2* expression in the brain and eye was very similar to that for *Olfm1* (Nakaya et al., 2013).

Functional and morphological changes in the eyes of Olfm2-KO^{LacZ} mice

Since a mutation in the *OLFM2* gene was found to be associated with primary open-angle glaucoma in Japanese patients (Funayama et al., 2006), we analyzed functional and morphological changes in the eyes of *Olfm2*-KO^{LacZ} animals. First, we measured intraocular pressure in 2–8 month-old mice. No differences were found between *Olfm*-KO^{LacZ} and their WT littermates (data not shown).

To assess functional changes, we performed simultaneous ERG and VEP recordings using 5 pairs of 8–12 month-old WT and *Olfm2*-KO^{LacZ} littermates. For photopic ERG, there are no differences in b-wave amplitudes and peak time for responses recorded from *Olfm2*-KO^{LacZ} compared with WT littermates (Fig. 4C, D). However, VEP recording showed a significant reduction in the amplitude of the first negative wave (n1), the primary wave at the visual cortex evoked by an illuminative input to the eyes, in *Olfm2*-KO^{LacZ} as compared with their WT littermates (Fig. 4A, B). No differences in the peak times for the n1 wave were detected between *Olfm2*-KO^{LacZ} and WT littermates (Fig. 4A, B).

To assess whether the number of axons, axon degeneration and myelination are affected by the loss of *Olfm2*, we compared optic nerves of *Olfm2*-KO^{LacZ} and WT littermates. Analysis of semithin sections of the optic nerve from 8 month-old animals showed a slight reduction (about 8%) in the total number of axons in *Olfm2*-KO^{LacZ} mice as compared with WT littermates (Fig. 4E). Whole mount staining of the retina with Brn3 and NeuN antibodies also showed a slight reduction in the number of RGCs (Fig. 4F). However, these differences were not statistically significant in either case ($p = 0.19$ and 0.065, respectively). No significant differences in the number of axons between WT and *Olfm2*-KO^{LacZ} animals were detected when transverse sections of the optic nerve were analyzed by electron microscopy (Fig. 4E). However, myelin sheath looked less compact in *Olfm2*-KO^{LacZ} than in WT littermates at higher magnification (Fig. 4G). We concluded that functional changes detected in the eyes in *Olfm2*-KO^{LacZ} mice occurred without gross morphological changes in their eyes as compared with WT littermates.

Mouse behavioral tests

Our previous results demonstrated that a deletion in the *Olfm1* gene encoding 52 amino acids in the central part of the protein molecule leads to changes in behavior and social activity (Nakaya et al., 2013). Therefore, we performed several behavioral tests using *Olfm2*-KO^{LacZ} and their WT littermates. The anxiety of KO mice was first tested in an elevated plus maze. Five pairs of KO and WT littermates ranging in age from 5 to 8 months were used in this test. *Olfm2*-KO^{LacZ} animals spent more time on the open arms of the maze and made more entries into the open arms as compared with their WT littermates but these differences were not statistically significant (Fig. 5A, B). Anxiety behavior was also analyzed using the marble-burying test. This test showed no difference between *Olfm2*-

KO^{LacZ} and WT littermates (not shown). The open field test was used to measure locomotion and anxiety related behavior in 9 WT and 8 *Olfm2*-KO^{LacZ} animals ranging in age from 2 to 8 months. *Olfm2*-KO^{LacZ} mice spent test time preferentially in the light area, while their WT littermates spent test time preferentially in the dark area (Fig. 5C). Distance traveled by *Olfm2*-KO^{LacZ} mice in the dark and light compartment and the total distance during 10 minutes of test duration was significantly reduced as compared with their WT littermates (Fig. 5D, E). A decrease in the rearing frequency along with decreased rearing intervals was also found in *Olfm2*-KO^{LacZ} animals as compared with their WT littermates (Fig. 5F, G). To analyze a motor coordination, we performed a rotarod test at three consecutive days. *Olfm2*-KO^{LacZ} showed a reduced motor coordination compared with their WT littermates at time points tested but it reached statistically significant values only at day 2 (Fig. 5H). Finally, we examined the olfactory functions of *Olfm2*-KO^{LacZ} mice and their WT littermates by a simple smell test. *Olfm2*-KO^{LacZ} mice spent significantly less time exploring social odors (urine and cage wipe) as compared with their WT littermates. *Olfm2*-KO^{LacZ} mice also showed a slight decrease in the exploratory time with peanut butter but this decrease was not statistically significant (Fig. 5I). We concluded that *Olfm2*-KO^{LacZ} mice, similar to *Olfm1* mutant mice, showed reduced levels of exploratory and locomotor activities as well as changes in the olfactory functions. In addition, *Olfm2*-KO^{LacZ} mice showed reduced motor coordination on the rotarod test which did not reach statistically significant values for *Olfm1* mutant mice (Nakaya et al., 2013). Similar behavioral changes in the *Olfm1* mutant and *Olfm2* KO mice might suggest that these proteins play similar roles in behavior control.

Co-localization of Olfm2 protein with the AMPA receptor in the synaptosomal membrane fraction and its interaction with GluR2

Olfm1 and Olfm2 are able to form heterodimers and available data suggest that they may perform similar functions (Sultana et al., 2011). Shotgun analysis of proteins constituting the AMPAR complexes demonstrated that Olfm1 and Olfm2 are the components of these complexes (Schwenk et al., 2012, Shanks et al., 2012). Our results also confirmed that Olfm1 interacts with the AMPAR complexes (Nakaya et al., 2013). Since details of Olfm2 interaction with AMPAR are not known, we tested how a deletion of Olfm2 may affect the composition of the AMPAR complex.

It has been shown that the GluR1-4 subunits of the AMPAR complex are located in the light membrane and crude and pure synaptic membrane fractions (P3, P2 and LP1, respectively) upon biochemical fractionation (Lee et al., 2001, Hallett et al., 2008). Subcellular fractionation of the cortex and retina demonstrated that Olfm2 and Olfm1, similar to GluR2, co-purified with synaptic marker PSD95 in LP1 (Fig. 6A). The loss of Olfm2 results in increased levels of Olfm1, GluR2 and GluR3 and decreased level of CNIH2 in the LP1 fraction from the cortex of 4 month-old *Olfm2*-KO^{LacZ} KO mice as compared with WT littermates (Fig. 6B, C). No significant differences in the levels of GluR1, pGluR2, GluR4, PSD95, synaptophysin, synaptogyrin3, and PRCα were detected.

The LP1 fractions from cortex lysates of *Olfm2*-KO^{LacZ} and WT mice was used for immunoprecipitation with antibodies against GluR2, the major subunit of AMPAR in the

cortex, and immunoprecipitates were probed with antibodies against Olfm2, Olfm1, PSD95, CNIH2, GluR2 and GluR4. The results of immunoprecipitation confirmed that Olfm2 interacts with AMPAR. They also demonstrated increased level of GluR2 and reduced levels of Olfm1, PSD95, and CNIH2 in the AMPA receptor complex of *Olfm2*-KO^{LacZ} as compared with WT mice (Fig. 6D, E). The antibodies against Olfm2 were not efficient in immunoprecipitation experiments and hence we were not able to perform reciprocal immunoprecipitation. However, the GluR2 subunit could be efficiently immunoprecipitated from lysates of HEK293 cells co-transfected with FLAG-tagged Olfm2 and GFP-tagged GluR2 (not shown). When polyclonal rabbit antibodies against Olfm1 were used for immunoprecipitation, the level of GluR2 was reduced in immunoprecipitates from the LP1 fraction of the cortex of *Olfm2*-KO^{LacZ} mice as compared with their WT littermates (Fig. 6F). Olfm1 and Olfm2 are able to form heterodimers (Sultana et al., 2011) and results of immunoprecipitation from the LP1 fraction suggest that heterodimers of Olfm1 and Olfm2 interacts with AMPAR more efficiently than Olfm1 or Olfm2 homodimers. We also concluded that a relative abundance of several proteins is different in the AMPAR complexes of *Olfm2*-KO^{LacZ} and WT mice.

Discussion

Olfm2 is one of the most conserved members of the family of olfactomedin domain-containing proteins showing 96% identity in the amino acid sequence between human and mouse. Although the functions of olfactomedin domain-containing proteins are not well understood, it is now well established that mutations in genes encoding some of them may lead to human pathologies. So, mutations in the *MYOCILIN* (*MYOC*) gene may lead to juvenile primary open and adult onset glaucoma (Adam et al., 1997, Stone et al., 1997). Mutations in the *LPHN2* gene may be drivers of lung cancer tumorigenesis (Zheng et al., 2013), while mutations in the *LPHN3* gene were associated with attention-deficit/ hyperactivity disorder (Arcos-Burgos et al., 2010). Mutations in *OLFM2* leading to R144Q and T86M changes in the amino acid sequence were implicated in open-angle glaucoma in Japanese patients (Funayama et al., 2006) and colorectal cancer (Wood et al., 2007), respectively.

In the present study, we investigated effects of the *Olfm2* null mutation and demonstrated that *Olfm2*-KO^{LacZ} mice did not show gross phenotypic defects and had normal life span. The absence of significant phenotypical changes has been also reported for several null mutations in other genes encoding olfactomedin domain-containing proteins. So far, *Olfm4* KO mice showed normal development, fertility, and viability but demonstrated significantly lower *H. pylori* colonization in the gastric mucosa relative to wild-type littermates (Liu et al., 2010). *Olfml3* null mutation in mice did not produce a clear phenotype and the homozygous mutants were born normal and fertile (Ikeya et al., 2005). *Lphn1* null were fertile and survived for more than 1 year. The only abnormality observed was that female KO mice were less able to attend to litters than WT mice (Tobaben et al., 2002). Finally, although *Myoc* null mice demonstrated defects in myelination of sciatic and optic nerves (Kwon et al., 2013a, Kwon et al., 2014) and reduced cortical bone thickness and trabecular volume compared with wild-type mice (Kwon et al., 2013b), these mice did not develop glaucoma (Kim et al., 2001). Similarly, it has been reported that elderly woman homozygous

for the Arg46Stop mutation in myocilin did not develop glaucoma (Lam et al., 2000). Altogether, these data may suggest that functions of olfactomedin domain-proteins are dispensable or compensated by other redundant members of the family. In the case of Olfm2, Olfm1 or Olfm3 may represent such redundant members. These three proteins belong to the same subfamily I, show an overlapping expression pattern and the highest identity to each other compared with other family members. Indeed, our preliminary data show that *Olfm2* null mice that are also homozygous for the *Olfm1* mutation with a deletion of 52 amino acids in the central part of the protein molecule (Nakaya et al., 2013) have more severe phenotype than *Olfm2* or *Olfm1* single mutants and most double mutant mice die within one day after birth (Sultana et al., in preparation). It should be mentioned that knockdown of *olfm2* expression in zebrafish using morpholino oligonucleotides leads to more pronounced defects than *Olfm2* null mutation in mice. Interference with olfm2 expression resulted in impaired development of branchiomotor neurons, specific disruption of the late phase branchiomotor axon guidance, and affected development of the caudal pharyngeal arches, olfactory pits, eyes and optic tectum (Lee et al., 2008). These discrepancies in morphological defects between mice and zebrafish could be explained by species differences. Another explanation is that there are more and more examples in literature that morpholino oligonucleotide injection produce more pronounced phenotype than genetic knockout within the same species (zebrafish) (Eisen and Smith, 2008), indicating that morpholino injection may lead to additional unspecific effects even when multiple controls are included.

Although *Olfm2*-KO^{LacZ} did not show gross defects, *Olfm2* expression in the eye and brain stimulated a more careful investigation of potential ocular and behavioral abnormalities. *Olfm2*-KO^{LacZ} had normal intraocular pressure. However, *Olfm2*-KO^{LacZ} mice demonstrated a slight decrease in the number of RGCs and changes in the compactness of myelin sheath. Loss of RGCs may lead to changes in synaptic connectivity resulting in a decrease in the amplitude on a VEP test. Indeed, *Olfm2*-KO^{LacZ} showed a decrease in the first negative wave amplitude as compared with their WT littermates using a VEP test (Fig. 4A–B). A similar decrease in the first wave amplitude has been reported in a DBA/2J glaucomatous mouse model and in an OPA1-associated autosomal dominant optic atrophy model (Heiduschka et al., 2010, Sullivan et al., 2011). Slight reduction of the compactness of myelin sheath was not sufficient to change the peak time of the VEP response. VEP characterizes electrical response of the visual cortex to a visual stimulus and depends upon functionally intact visual pathway from the retina to primary visual cortex. Since *Olfm2* is expressed in the visual cortex, changes in the visual cortex as a result of *Olfm2* KO also may contribute to the observed changes in the VEP amplitude.

Olfm2-KO^{LacZ} mice showed moderate behavioral changes that were less pronounced than the ones observed in mice expressing mutated Olfm1 with a deletion of 52 amino acids in the central part of the protein molecule (Nakaya et al., 2013). This could be due to the fact that the level of *Olfm1* expression is significantly higher than the level of *Olfm2* expression in both the eye and brain (Sultana et al., 2011). In addition, Olfm1 mutant may act as a dominant negative mutant leading to a more severe phenotype. *Olfm2*-KO^{LacZ} mice demonstrated abnormal anxiety in open field and elevated maze tests spending more time in

the light compartment or open arm area, respectively. *Olfm2*-KO^{LacZ} mice also showed reduced locomotion as judged by open field and rotarod tests compared with their WT littermates.

Olfm2 KO leads to the elevation of Olfm1 level in the LP1 fraction from the cortex of *Olfm2*-KO^{LacZ} as compared with WT mice supporting the idea of a mutual compensatory role of olfactomedin domain-containing proteins. In addition, the levels of GluR2 and GluR3 were increased while the level of CNIH2 was decreased in the LP1 fraction of *Olfm2* KO as compared with WT mice. At the same time, the level of Olfm1 was reduced in the AMPAR complexes isolated from the LP1 fraction of *Olfm2* KO mice by immunoprecipitation with antibodies against GluR2 as compared with WT samples. Similarly, the level of Olfm2 was slightly reduced in the AMPAR complexes of the mouse cortex expressing mutated Olfm1 with a deletion in the central part as compared with WT samples (Sultana et al., in preparation). These data suggests that heterodimers of Olfm1 and Olfm2 interact more efficiently with AMPAR than homodimers of Olfm1 or Olfm2. Immunoprecipitation from the LP1 fraction of *Olfm2* KO mice cortex also showed reduced interaction of GluR2 with PSD95 and CNIH2 as compared with WT mice. Although it has been shown that properties of the AMPAR complexes may be affected by the composition of complexes, we still do not know how electrophysiological properties of these complexes are modified by the interaction with Olfm1 and Olfm2 heterodimers. Nevertheless our data suggest that Olfm2, as well as Olfm1, affect the composition of the AMPAR complexes at least in the cortex and may play an important role at the synapses and in synapse-related functions.

Acknowledgments

We thank Yichao Li for his help with ERG and VEP recording.

This work was supported by the Intramural Research Programs of the National Eye Institute, National Institutes of Health.

Abbreviations

EMT	elevated plus maze test
ERG	electroretinogram
KO	knockout
Olfm2	olfactomedin 2
***Olfm2*-KO**	*Olfm2* knockout
β-gal	β-galactosidase
PFA	paraformaldehyde
Q-PCR	quantitative RT-PCR
RGC	retinal ganglion cell
VEP	visual evoked potential

WT wild-type

References

Adam MF, Belmouden A, Binisti P, Brezin AP, Valtot F, Bechetoille A, Dascotte JC, Copin B, Gomez L, Chaventre A, Bach JF, Garchon HJ. Recurrent mutations in a single exon encoding the evolutionarily conserved olfactomedin-homology domain of TIGR in familial open-angle glaucoma. Hum Mol Genet. 1997; 6:2091–2097. [PubMed: 9328473]

Arcos-Burgos M, Jain M, Acosta MT, Shively S, Stanescu H, Wallis D, Domene S, Velez JI, Karkera JD, Balog J, Berg K, Kleta R, Gahl WA, Roessler E, Long R, Lie J, Pineda D, Londono AC, Palacio JD, Arbelaez A, Lopera F, Elia J, Hakonarson H, Johansson S, Knappskog PM, Haavik J, Ribases M, Cormand B, Bayes M, Casas M, Ramos-Quiroga JA, Hervas A, Maher BS, Faraone SV, Seitz C, Freitag CM, Palmason H, Meyer J, Romanos M, Walitza S, Hemminger U, Warnke A, Romanos J, Renner T, Jacob C, Lesch KP, Swanson J, Vortmeyer A, Bailey-Wilson JE, Castellanos FX, Muenke M. A common variant of the latrophilin 3 gene, LPHN3, confers susceptibility to ADHD and predicts effectiveness of stimulant medication. Mol Psych. 2010; 15:1053–1066.

Basta-Kaim A, Fijal K, Budziszewska B, Regulska M, Leskiewicz M, Kubera M, Golembiowska K, Lason W, Wedzony K. Prenatal lipopolysaccharide treatment enhances MK-801-induced psychotomimetic effects in rats. Pharmacol Biochem Behav. 2011; 98:241–249. [PubMed: 21236292]

Cheng A, Arumugam TV, Liu D, Khatri RG, Mustafa K, Kwak S, Ling HP, Gonzales C, Xin O, Jo DG, Guo Z, Mark RJ, Mattson MP. Pancortin-2 interacts with WAVE1 and Bcl-xL in a mitochondria-associated protein complex that mediates ischemic neuronal death. J Neurosci. 2007; 27:1519–1528. [PubMed: 17301160]

Danielson PE, Forss-Petter S, Battenberg EL, deLecea L, Bloom FE, Sutcliffe JG. Four structurally distinct neuron-specific olfactomedin-related glycoproteins produced by differential promoter utilization and alternative mRNA splicing from a single gene. J Neurosci Res. 1994; 38:468–478. [PubMed: 7932877]

Eisen JS, Smith JC. Controlling morpholino experiments: don’t stop making antisense. Dev. 2008; 135:1735–1743.

Funayama T, Mashima Y, Ohtake Y, Ishikawa K, Fuse N, Yasuda N, Fukuchi T, Murakami A, Hotta Y, Shimada N. SNPs and interaction analyses of noelin 2, myocilin, and optineurin genes in Japanese patients with open-angle glaucoma. Invest Ophthalmol Vis Sci. 2006; 47:5368–5375. [PubMed: 17122126]

Hallett PJ, Collins TL, Standaert DG, Dunah AW. Biochemical fractionation of brain tissue for studies of receptor distribution and trafficking. Cur Protocols Neurosci. 2008; Chapter 1(Unit 1.16)

Heiduschka P, Schnichels S, Fuhrmann N, Hofmeister S, Schraermeyer U, Wissinger B, Alavi MV. Electrophysiological and histologic assessment of retinal ganglion cell fate in a mouse model for OPA1-associated autosomal dominant optic atrophy. Invest Ophthalmol Vis Sci. 2010; 51:1424–1431. [PubMed: 19834041]

Ikeya M, Kawada M, Nakazawa Y, Sakuragi M, Sasai N, Ueno M, Kiyonari H, Nakao K, Sasai Y. Gene disruption/knock-in analysis of mONT3: vector construction by employing both in vivo and in vitro recombinations. Int J Dev Biol. 2005; 49:807–823. [PubMed: 16172977]

Kim BS, Savinova OV, Reedy MV, Martin J, Lun Y, Gan L, Smith RS, Tomarev SI, John SW, Johnson RL. Targeted disruption of the Myocilin gene (Myoc) suggests that human glaucoma-causing mutations are gain of function. Mol Cell Biol. 2001; 21:7707–7713. [PubMed: 11604506]

Kulkarni NH, Karavanich CA, Atchley WR, Anholt RR. Characterization and differential expression of a human gene family of olfactomedin-related proteins. Genet Res. 2000; 76:41–50. [PubMed: 11006633]

Kwon HS, Johnson TV, Joe MK, Abu-Asab M, Zhang J, Chan CC, Tomarev SI. Myocilin mediates myelination in the peripheral nervous system through ErbB2/3 signaling. J Biol Chem. 2013a; 288:26357–26371. [PubMed: 23897819]

Kwon HS, Johnson TV, Tomarev SI. Myocilin stimulates osteogenic differentiation of mesenchymal stem cells through MAPK signaling. J Biol Chem. 2013b; 288:16882–16894. [PubMed: 23629661]

Kwon HS, Nakaya N, Abu-Asab M, Kim HS, Tomarev SI. Myocilin is involved in NgR1/Lingo-1-mediated oligodendrocyte differentiation and myelination of the optic nerve. J Neurosci. 2014; 34:5539–5551. [PubMed: 24741044]

Lam DS, Leung YF, Chua JK, Baum L, Fan DS, Choy KW, Pang CP. Truncations in the TIGR gene in individuals with and without primary open-angle glaucoma. Invest Ophthalmol Vis Sci. 2000; 41:1386–1391. [PubMed: 10798654]

Lee JA, Anholt RR, Cole GJ. Olfactomedin-2 mediates development of the anterior central nervous system and head structures in zebrafish. Mech Dev. 2008; 125:167–181. [PubMed: 18037275]

Lee SH, Valtschanoff JG, Kharazia VN, Weinberg R, Sheng M. Biochemical and morphological characterization of an intracellular membrane compartment containing AMPA receptors. Neuropharmacol. 2001; 41:680–692.

Lewandoski M, Wassarman KM, Martin GR. Zp3-cre, a transgenic mouse line for the activation or inactivation of loxP-flanked target genes specifically in the female germ line. Curr Biol. 1997; 7:148–151. [PubMed: 9016703]

Lister RG. The use of a plus-maze to measure anxiety in the mouse. Psychopharmacol. 1987; 92:180–185.

Liu W, Yan M, Liu Y, Wang R, Li C, Deng C, Singh A, Coleman WG Jr, Rodgers GP. Olfactomedin 4 down-regulates innate immunity against Helicobacter pylori infection. Proc Natl Acad Sci USA. 2010; 107:11056–11061. [PubMed: 20534456]

Mead AN, Morris HV, Dixon CI, Rulten SL, Mayne LV, Zamanillo D, Stephens DN. AMPA receptor GluR2, but not GluR1, subunit deletion impairs emotional response conditioning in mice. Behav Neurosci. 2006; 120:241–248. [PubMed: 16719688]

Michalska AE, Choo KH. Targeting and germ-line transmission of a null mutation at the metallothionein I and II loci in mouse. Proc Natl Acad Sci USA. 1993; 90:8088–8092. [PubMed: 8367468]

Nagano T, Nakamura A, Konno D, Kurata M, Yagi H, Sato M. A2-Pancortins (Pancortin-3 and -4) are the dominant pancortins during neocortical development. J Neurochem. 2000; 75:1–8. [PubMed: 10854240]

Nakaya N, Lee HS, Takada Y, Tzchori I, Tomarev SI. Zebrafish olfactomedin 1 regulates retinal axon elongation in vivo and is a modulator of Wnt signaling pathway. J Neurosci. 2008; 28:7900–7910. [PubMed: 18667622]

Nakaya N, Sultana A, Lee HS, Tomarev SI. Olfactomedin 1 interacts with the nogo a receptor complex to regulate axon growth. J Biol Chem. 2012; 287:37171–37184. [PubMed: 22923615]

Nakaya N, Sultana A, Munasinghe J, Cheng A, Mattson MP, Tomarev SI. Deletion in the N-terminal half of olfactomedin 1 modifies its interaction with synaptic proteins and causes brain dystrophy and abnormal behavior in mice. Exp Neurol. 2013; 250:205–218. [PubMed: 24095980]

Park SK, Nguyen MD, Fischer A, Luke MP, el Affar B, Dieffenbach PB, Tseng HC, Shi Y, Tsai LH. Par-4 links dopamine signaling and depression. Cell. 2005; 122:275–287. [PubMed: 16051151]

Schwenk J, Harmel N, Brechet A, Zolles G, Berkefeld H, Muller CS, Bildl W, Baehrens D, Huber B, Kulik A, Klocker N, Schulte U, Fakler B. High-resolution proteomics unravel architecture and molecular diversity of native AMPA receptor complexes. Neuron. 2012; 74:621–633. [PubMed: 22632720]

Shanks NF, Savas JN, Maruo T, Cais O, Hirao A, Oe S, Ghosh A, Noda Y, Greger IH, Yates JR 3rd, Nakagawa T. Differences in AMPA and kainate receptor interactomes facilitate identification of AMPA receptor auxiliary subunit GSG1L. Cell Rep. 2012; 1:590–598. [PubMed: 22813734]

Stone EM, Fingert JH, Alward WL, Nguyen TD, Polansky JR, Sunden SL, Nishimura D, Clark AF, Nystuen A, Nichols BE, Mackey DA, Ritch R, Kalenak JW, Craven ER, Sheffield VC. Identification of a gene that causes primary open angle glaucoma. Science. 1997; 275:668–670. [PubMed: 9005853]

Sullivan TA, Geisert EE, Hines-Beard J, Rex TS. Systemic adeno-associated virus-mediated gene therapy preserves retinal ganglion cells and visual function in DBA/2J glaucomatous mice. Hum Gene Ther. 2011; 22:1191–1200. [PubMed: 21542676]

Sultana A, Nakaya N, Senatorov VV, Tomarev SI. Olfactomedin 2: Expression in the eye and interaction with other olfactomedin domain-containing proteins. Invest Ophthalmol Vis Sci. 2011; 52:2584–2592. [PubMed: 21228389]

Thomas A, Burant A, Bui N, Graham D, Yuva-Paylor LA, Paylor R. Marble burying reflects a repetitive and perseverative behavior more than novelty-induced anxiety. Psychopharmacol. 2009; 204:361–373.

Tobaben S, Sudhof TC, Stahl B. Genetic analysis of alpha-latrotoxin receptors reveals functional interdependence of CIRL/latrophilin 1 and neurexin 1 alpha. J Biol Chem. 2002; 277:6359–6365. [PubMed: 11741895]

Tomarev SI, Nakaya N. Olfactomedin domain-containing proteins: possible mechanisms of action and functions in normal development and pathology. Mol Neurobiol. 2009; 40:122–138. [PubMed: 19554483]

Torrado M, Trivedi R, Zinovieva R, Karavanova I, Tomarev SI. Optimedin: a novel olfactomedin-related protein that interacts with myocilin. Hum Mol Genet. 2002; 11:1291–1301. [PubMed: 12019210]

Witt RM, Galligan MM, Despinoy JR, Segal R. Olfactory behavioral testing in the adult mouse. J Vis Exp. 2009; 23

Wood LD, Parsons DW, Jones S, Lin J, Sjoblom T, Leary RJ, Shen D, Boca SM, Barber T, Ptak J, Silliman N, Szabo S, Dezso Z, Ustyanksky V, Nikolskaya T, Nikolsky Y, Karchin R, Wilson PA, Kaminker JS, Zhang Z, Croshaw R, Willis J, Dawson D, Shipitsin M, Willson JK, Sukumar S, Polyak K, Park BH, Pethiyagoda CL, Pant PV, Ballinger DG, Sparks AB, Hartigan J, Smith DR, Suh E, Papadopoulos N, Buckhaults P, Markowitz SD, Parmigiani G, Kinzler KW, Velculescu VE, Vogelstein B. The genomic landscapes of human breast and colorectal cancers. Science. 2007; 318:1108–1113. [PubMed: 17932254]

Zeng LC, Han ZG, Ma WJ. Elucidation of subfamily segregation and intramolecular coevolution of the olfactomedin-like proteins by comprehensive phylogenetic analysis and gene expression pattern assessment. FEBS Lett. 2005; 579:5443–5453. [PubMed: 16212957]

Zheng CX, Gu ZH, Han B, Zhang RX, Pan CM, Xiang Y, Rong XJ, Chen X, Li QY, Wan HY. Whole-exome sequencing to identify novel somatic mutations in squamous cell lung cancers. Int J Oncol. 2013; 43:755–764. [PubMed: 23799614]

Highlights

- *Olfactomedin 2* (*Olfm2*) gene is actively expressed in neuronal tissues.
- *Olfm2* null mice showed abnormalities in various behavioral tests.
- Olfm2 interacts with the GluR2 subunit of the AMPAR complexes.
- Elimination of Olfm2 resulted in a modification of the AMPAR complex.
- Olfm2 plays a role in the organization of the AMPA receptor complexes.

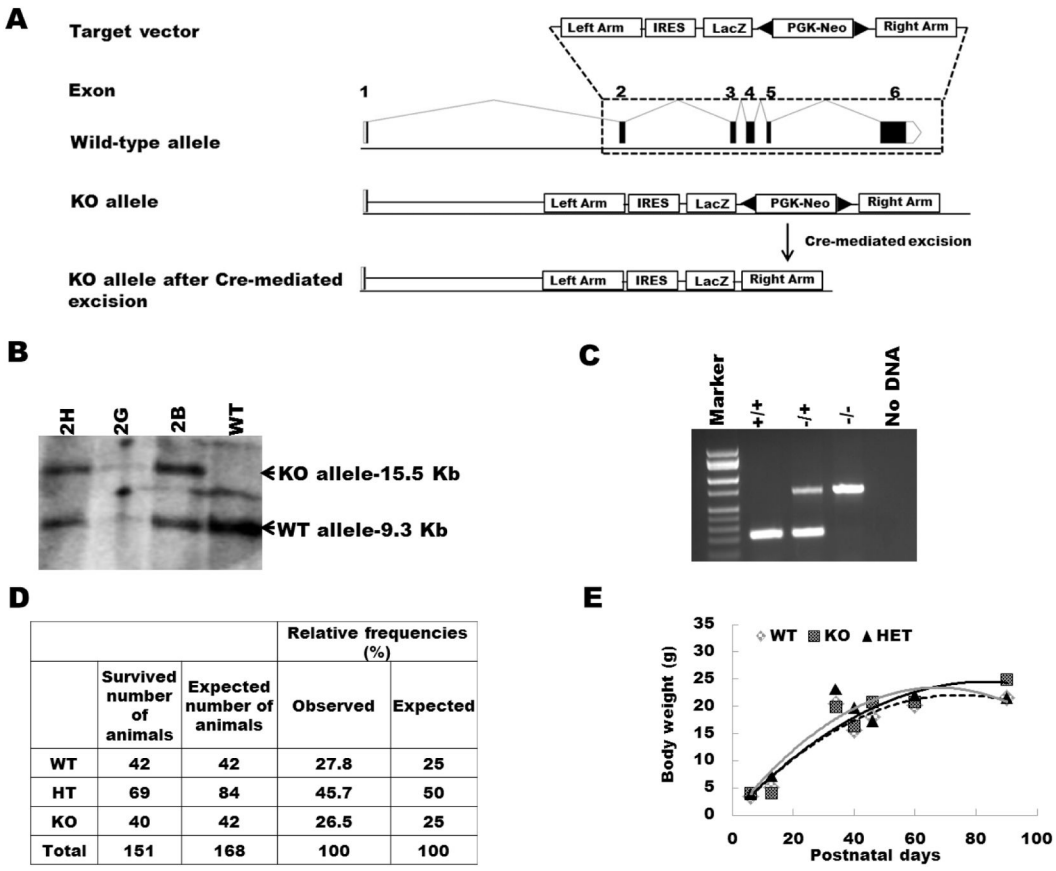

			Relative frequencies (%)	
	Survived number of animals	Expected number of animals	Observed	Expected
WT	42	42	27.8	25
HT	69	84	45.7	50
KO	40	42	26.5	25
Total	151	168	100	100

Fig. 1.

Generation of *Olfm2*-KO^{LacZ} mice. **A.** The gene targeting strategy of the mouse *Olfm2* gene. The *Olfm2* gene consists of 6 exons shown as filled boxes. Exons 2–6 were replaced with the LacZ and PGK neo cassette using homologous recombination. Black triangles in the target vector and *Olfm2*-KO allele correspond to the loxP sites. **B.** Southern blot analysis of positive ES clones (2H, 2G, 2B) and WT control. Genomic DNA was cleaved with the ScaI restriction endonuclease and tested with the 5′-flanking probe. Restriction fragments of 9.3 kb and 15.5 kb correspond to WT and KO alleles, respectively. **C.** PCR genotyping of wild-type (+/+), heterozygous (+/−) and homozygous (−/−) *Olfm2*-KO^{LacZ} mice. **D.** Expected and observed frequencies of mice surviving until weaning at 3 weeks after mating heterozygous *Olfm2*-KO^{LacZ} mice. **E.** Body weight of WT, heterozygous, and homozygous *Olfm2*-KO^{LacZ} animals at different postnatal ages.

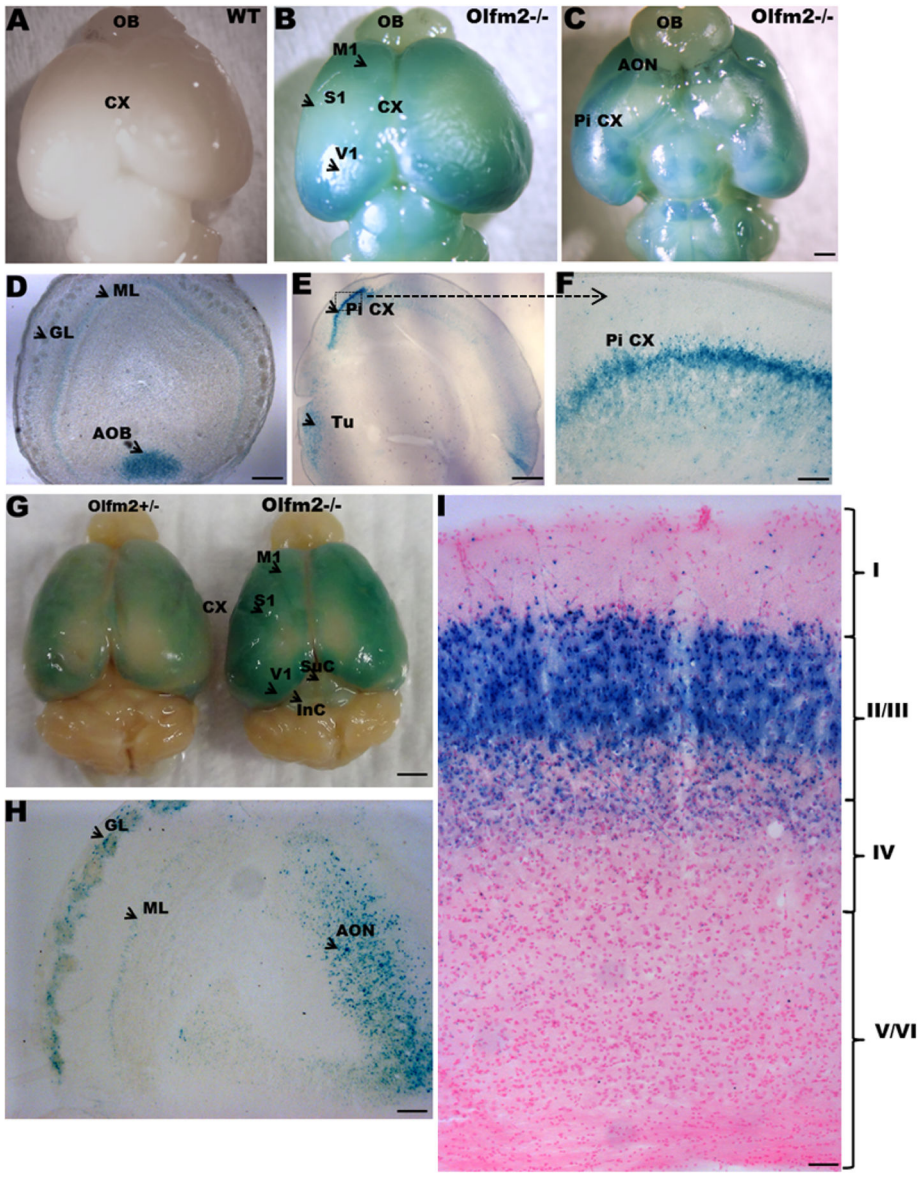

Fig. 2.

Olfm2 expression in the brain as seen by X-gal staining. **A–C.** Whole mount X-gal staining of P5 WT and homozygous *Olfm2*-KO^{LacZ} mouse brain shown from dorsal (**A–B**) and ventral (**C**) sides. The arrowheads in **B** mark the expression in the motor cortex (M1), somatosensory cortex (S1), and visual cortex (V1). On the ventral side (**C**), expression is mainly seen in the accessory olfactory nuclei (AON) and piriform cortex. **D.** Section of the P5 olfactory bulb showing the expression in the glomeruli (GL), mitral layer (ML), and accessory olfactory bulb (AOB). **E.** Section of the P5 developing cortex showing expression in the piriform cortex (Pi CX) and olfactory trabeculae (Tu). **F.** Higher magnification of expression seen in the piriform cortex. **G.** *Olfm2* expression in the brain of adult heterozygous and homozygous *Olfm2*-KO^{LacZ} mice. The arrowheads indicate the expression in the motor cortex (M1), somatosensory cortex (S1), and visual cortex (V1). **H.** Coronal

section of the adult olfactory bulb showing *Olfm2* expression in the glomeruli (GL), mitral layer (ML), and anterior olfactory nuclei (AON). **I.** Coronal section of the adult cortex showing *Olfm2* expression in cortical layers II, III and weak expression extending into layer IV. Scale bars: 1 mm in **A–C**, 200 μm in **D–E**, 100 μm in **F, H–I**, and 2 mm in **G**.

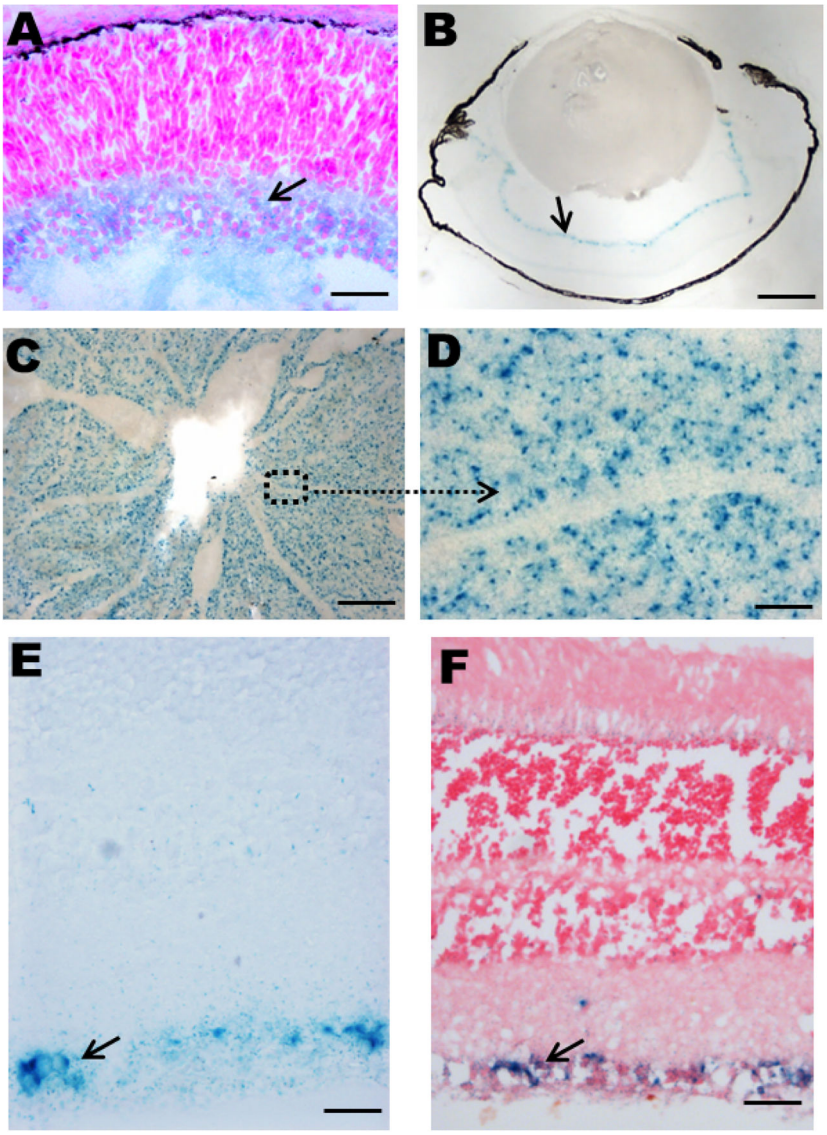

Fig. 3.

Expression of *Olfm2* in the eye as seen by X-gal staining. **A.** X-gal staining of developing eye at embryonic day 18. The section was counter stained with nuclear fast red stain. Expression at this stage is seen in differentiating RGCs marked by arrow. **B.** Section of the P13 mouse eye. *Olfm2* expression was detected mainly in the RGC layer (arrow). **C.** Whole mount X-gal staining of adult retina. **D.** Higher magnification of the area that was boxed in **C. E.** Section of adult retina. *Olfm2* expression was detected in the RGC layer (arrow). **F.** Section as in **E** was counter stained with nuclear fast red stain. Scale bars: 50 μm in **A**, **D**, **E** and **F**; 200 μm in **B** and **C**.

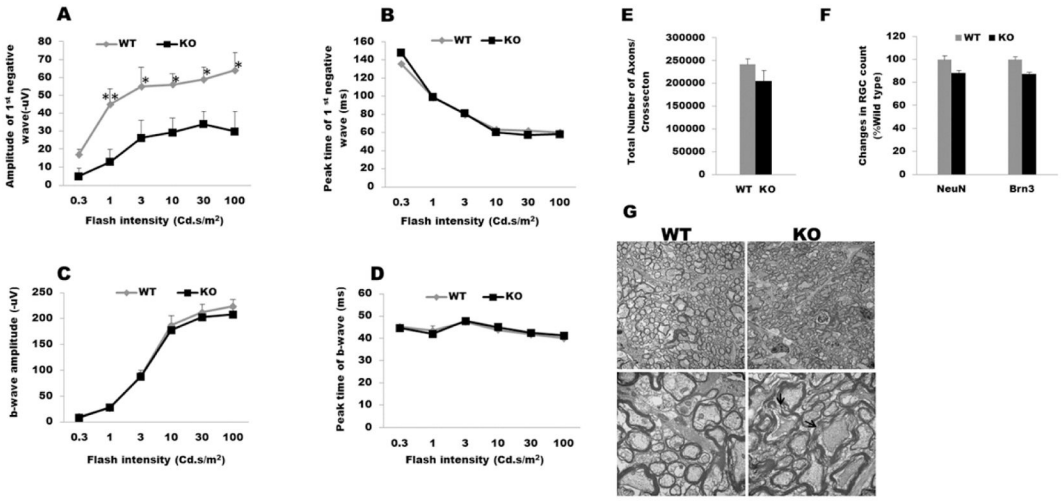

Fig. 4.

Functional changes in the eye *Olfm2*-KO^{LacZ} mice. **A–B.** The first negative wave amplitude (**A**) and peak time (**B**) of VEP recorded using *Olfm2*-KO^{LacZ} and WT littermates. **C–D.** The b-wave amplitude (**C**) and peak time (**D**) of photopic ERG recorded using *Olfm2*-KO^{LacZ} and WT littermates. Five pairs of animals were analyzed for each test (*p<0.05; **p<0.01). (E) The axon number in the optic nerve of 8 month-old *Olfm2*-KO^{Lacz} and WT littermates (n = 3). Semithin sections of the optic nerve were used for axon counting. **F.** Changes in the relative amount of Brn3 and NeuN positive RGCs in 8 month-old *Olfm2* KO ^{LacZ} compared with their WT littermates as detected by whole mount retinal staining. **G.** Electron micrographs of the optic nerve cross sections from WT and *Olfm2*-KO^{LacZ} mice. Typical images are shown. Arrow shows a reduced compactness of myelin in *Olfm2*-KO^{LacZ} mice showed as compared with their WT littermates. Upper panels Scale bars: 2 μm for the upper panels and 500 nm for the lower panels.

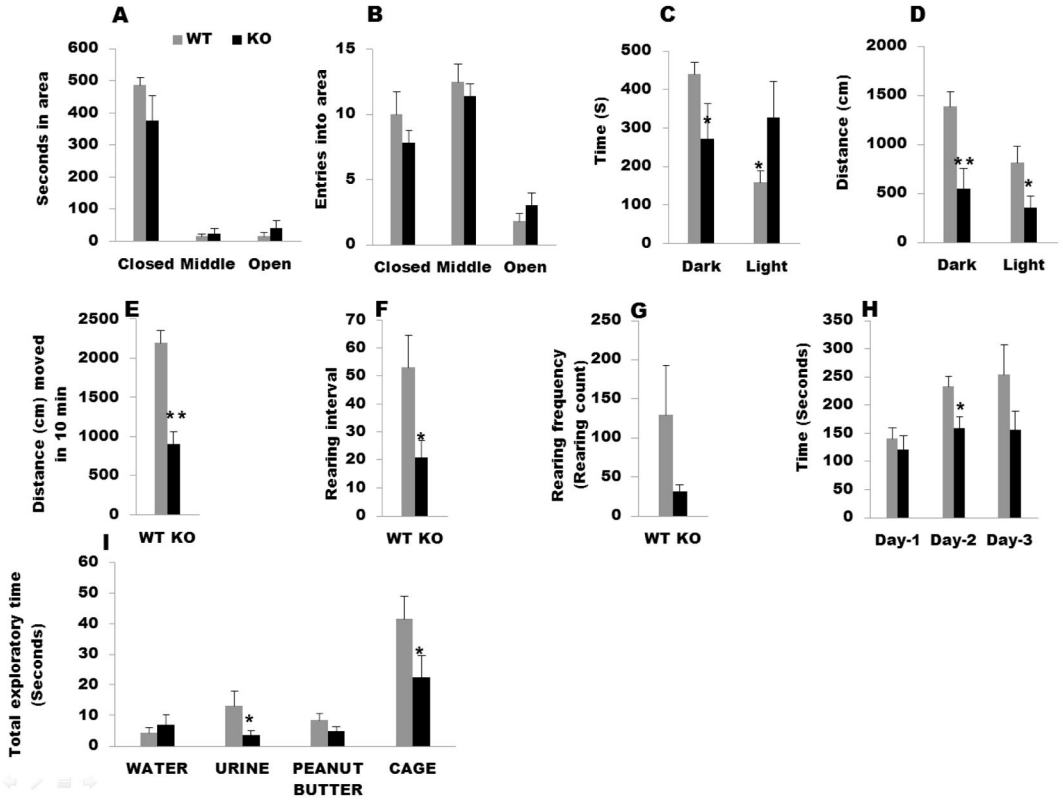

Fig. 5.

Olfm2-KO^{LacZ} mice exhibit locomotor and anxiety-related behavioral abnormalities. **A**. The elevated plus-maze test. Time spent in each area was measured during 10 min. n = 5 for each group. **B**. The number of entries into different arms of maze was measured during 10 min. **C**. Time spent in the light and dark compartments during 10 min are shown. Only mice that moved more than 100 cm in the open field test were selected for this test. n = 9 for WT and n = 8 for *Olfm2*-KO^{LacZ}. **D–E**. Average distance traveled in 10 min by WT (n = 9) and *Olfm2*-KO^{LacZ} (n = 8) in the light and dark compartments (**D**) as well as combined distance in both compartments (**E**). **F–G.** Rearing interval and frequency by WT and *Olfm2*-KO^{LacZ} mice during 10 minutes of test duration. **H**. The rotarod test. Average time during which WT (n = 6) and *Olfm2*-KO^{LacZ} (n = 6) littermates stayed on the rotating rod. The test was repeated for three consecutive days. **I**. Olfactory sensitivity test. WT mice (n=8) spent more time than their *Olfm2*-KO^{LacZ} littermates (n = 7) exploring social odors (urine and cage wipe) (*p<0.05; **p<0.01).

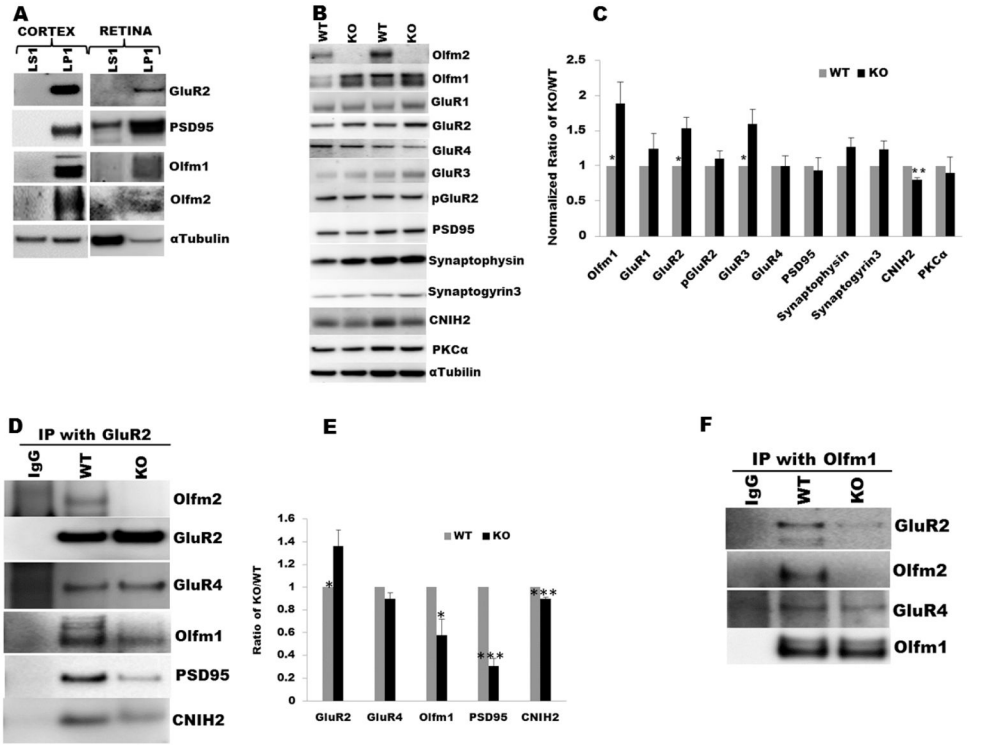

Fig. 6.

Co-localization and interaction of Olfm2 and Olfm1 with GluR2 in the synaptic membrane fraction (LP1). **A**. Biochemical fractionation of the cortex and retina showing co-purification of Olfm1, Olfm2, GluR2, and PSD95 with the LP1 fraction but not with the synaptic cytosol fraction (LS1). **B**. Western blots of the LP1 fraction from the cortex of WT and *Olfm2*-KO^{LacZ} mice. **C**. Quantification of 3 independent experiments as in **B**. The levels of Olfm1, GluR2 and GluR3 were significantly increased while the level of CNIH2 was significantly decreased in *Olfm2* KO as compared with WT samples. **D**. Co-immunoprecipitation of Olfm1, Olfm2, PSD95 with GluR2. Protein complexes were precipitated from the LP1 fraction of WT and *Olfm2*-KO^{LacZ} mouse cortex with anti-GluR2 antibody and analyzed by Western blot using indicated antibodies. Precipitation from WT cortex lysate with normal mouse IgG was used as a negative control. **E**. Quantification of 3 independent experiments as in **D. F**. Co-immunoprecipitation of GluR2 and Olfm2 with Olfm1. Protein complexes were precipitated from WT and *Olfm2*-KO^{LacZ} LP1 fractions of the mouse cortex with anti-Olfm1 antibody and analyzed by Western blot using indicated antibodies. Precipitation from WT cortex lysate with normal rabbit IgG was used as a negative control. (*p<0.05; **p<0.01; ***p<0.001)